Modification of Drop Shape Controlled by Electrowetting

Marguerite Bienia, Catherine Quilliet,* and Marcel Vallade

Laboratoire de Spectrométrie Physique, CNRS UMR n°5588, Université Joseph Fourier, BP87, 38402 Saint-Martin d'Hères Cedex, France

Received February 25, 2003. In Final Form: July 21, 2003

Wetting defects were created thanks to electrowetting: the effective surface tension between brine and an insulating solid is independently monitored, via an external electrical field, on two complementary areas (defect and background). This article describes the bicapacitor substrates that allow such a zone differentiation when connected to an adequate high-tension setup. Observations of the deformation of a drop on a stripe-shaped defect showed that it is possible to scan an appreciable range of wetting contrasts between the defect and the background with a unique sample. Theoretical calculations suggest an order of magnitude for electrostatic edge effects characteristic of these "virtual" wetting defects.

Introduction

Electrowetting (EW) on an insulator-coated electrode consists of applying a voltage between a drop of conducting liquid and a counter electrode, separated by a thin dielectric layer. This phenomenon results in a reduction of the contact angle between the liquid and the solid[1−5] up to saturation before reaching complete wetting, the nature of which is still under debate.[4,6−10] Modification of the contact angle, being mainly due to surface effects, is generally interpreted as a tuning of the effective solid/liquid surface tension by varying the applied potential. This made the displacement,[3,11] splitting, and merging[12] of drops of conducting liquids possible in devices without mechanical parts. More generally, electrical effects are known to allow efficient actuation of liquids, possibly through dielectrophoresis (DEP).[13,14] EW or DEP behavior depends on whether the liquids used have dielectric or conducting properties, this being triggered by the frequency of the applied field.[4,13]

We focused on modifying the shape of a drop by creating wetting defects controlled by EW. Besides actuation, controlling the shape of a drop may bring experimental solutions for studying more fundamental aspects of wetting, such as contact line relaxation[15] or the influence of defects on the contact angle hysteresis.[16−20] "Classical" wetting experiments are usually performed on samples with chemical or physical defects[21−27] obtained by chemical treatment or etching of the surface. The latter mixes the incidence of roughness and chemical nature of the substrate. The EW effect provides a control parameter for tuning the surface tension, the external electrical field, which does not alter the surface and may be decorrelated from the surface roughness. EW defects are expected, for a given defect geometry, to scan a large range of wetting contrasts between two zones as required by applying different electrical fields. For this purpose, we developed samples, which consisted of bilayered capacitors, where two distinct areas are controlled by two independent voltages. Subsequently, we call *background* the main area, and *defect* the minority area (see Figure 1). Before displaying the very first experiments performed on such defects, we will present theoretical calculations that forecast nontrivial effects related to the electrostatic nature of the driving forces.

* To whom correspondence should be addressed.

(1) Berge, B. Electrocapillarité et mouillage de films isolants par l'eau. *C. R. Acad. Sci., Ser. III* **1993**, *317*, 157.
(2) Quilliet, C.; Berge, B. Electrowetting: a recent outbreak. *Curr. Opin. Colloid Interface Sci.* **2001**, *6*, 34, and references therein.
(3) Prins, M. W. J.; Welters, W. J. J.; Weekamp, J. W. Fluid control in multichannel structures by electrocapillary pressure. *Science* **2001**, *291*, 277.
(4) Jones, T. B. On the relationship of dielectrophoresis and electrowetting. *Langmuir* **2002**, *18*, 4437.
(5) Kuo, J. S.; Spicar-Mihalic, P.; Rodriguez, I.; Chiu, D. T. Electrowetting-induced droplet movement in an immiscible medium. *Langmuir* **2003**, *19*, 250.
(6) Vallet, M.; Vallade, M.; Berge, B. Limiting phenomena for the spreading of water on polymer films by electrowetting. *Eur. Phys. J. B* **1999**, *11*, 583.
(7) Verheijen, H. J. J.; Prins, M. W. J. Reversible electrowetting and trapping of charge: model and experiments. *Langmuir* **1999**, *15*, 6616.
(8) Blake, T. D.; Clarke, A.; Stattersfield, E. H. An investigation of electrostatic assist in dynamic wetting. *Langmuir* **2000**, *16*, 2928.
(9) Seyrat, E.; Hayes, R. A. Amorphous fluoropolymers as insulators for reversible low-voltage electrowetting. *J. Appl. Phys.* **2001**, *90*, 1383.
(10) Shapiro, B.; Moon, H.; Garrell, R.; Kim, C. J. Equilibrium behavior of sessile drops under surface tension, applied external fields, and material variations. *J. Appl. Phys.* **2003**, *93*, 5794.
(11) Pollack, M. G.; Fair, R. B.; Sherendov, A. Electrowetting-based actuation of liquid microdroplets for microfluidic applications. *Appl. Phys. Lett.* **2000**, *77*, 1725.
(12) Berge, B. Unpublished results.
(13) Jones, T. B.; Gunji, M.; Washizu, M.; Feldman, M. J. Dielectrophoretic liquid actuation and nanodroplet formation. *J. Appl. Phys.* **2001**, *89*, 1441.
(14) Torkkeli, A.; Häärä, A.; Saarilahti, J.; Härmä, H.; Soukka, T.; Tolonen, P. Droplet manipulation on a superhydrophobic surface for microchemical analysis. *Transducers '01 Eurosensors XV*, Proceedings of the 11th international conference on solid-state sensors and actuators, Munich, Germany, June 10−14, 2001.
(15) Tanguy, A.; Gounelle, M.; Roux, S. From individual to collective pinning: effect of long-range elastic interactions. *Phys. Rev. E* **1998**, *58*, 1577.
(16) Schwartz, L. W.; Garoff, S. Contact angle hysteresis and the shape of the three-phase line. *J. Colloid Interface Sci.* **1985**, *106*, 422.
(17) Jansons, K. M. Moving contact lines on a two-dimensional rough surface. *J. Fluid Mech.* **1985**, *154*, 1.
(18) Pomeau, Y.; Vannimenus, J. Contact angle on heterogeneous surfaces: weak heterogeneities. *J. Colloid Interface Sci.* **1985**, *104*, 477.
(19) Robbins, M. O.; Joanny, J.-F. Contact angle hysteresis on random surfaces. *Europhys. Lett.* **1987**, *3*, 729.
(20) Raphaël, E.; De Gennes, P. G. Dynamics of wetting with nonideal surfaces. The single defect problem. *J. Chem. Phys.* **1989**, *90*, 7577.
(21) Johnson, R. E. J.; Dettre, R. H.; Brandreth, D. A. Dynamic contact angles and contact angle hysteresis. *J. Colloid Interface Sci.* **1977**, *62*, 205.
(22) Di Meglio, J.-M. Contact angle hysteresis and interacting surface defects. *Europhys. Lett.* **1992**, *17*, 607.
(23) De Jonghe, V.; Chatain, D. Experimental study of wetting hysteresis on surfaces with controlled geometrical and/or chemical defects. *Acta Metall. Mater.* **1995**, *43*, 1505.
(24) Ondarçuhu, T. Total or partial pinning of a droplet on a surface with a chemical discontinuity. *J. Phys. II (France)* **1995**, *5*, 227.
(25) Paterson, A.; Fermigier, M. Wetting on heterogeneous surfaces: influence of defects interactions. *Phys. Fluids* **1997**, *9*, 2210.
(26) Cubaud, T.; Fermigier, M.; Jenffer, P. Spreading of large drops on patterned surfaces. *Oil Gas Sci. Technol.* **2001**, *56*, 23.
(27) Ramos, S.; Charlaix, E. *Surf. Sci.*, in press.

10.1021/la030079w CCC: $25.00
Published on Web 09/27/2003

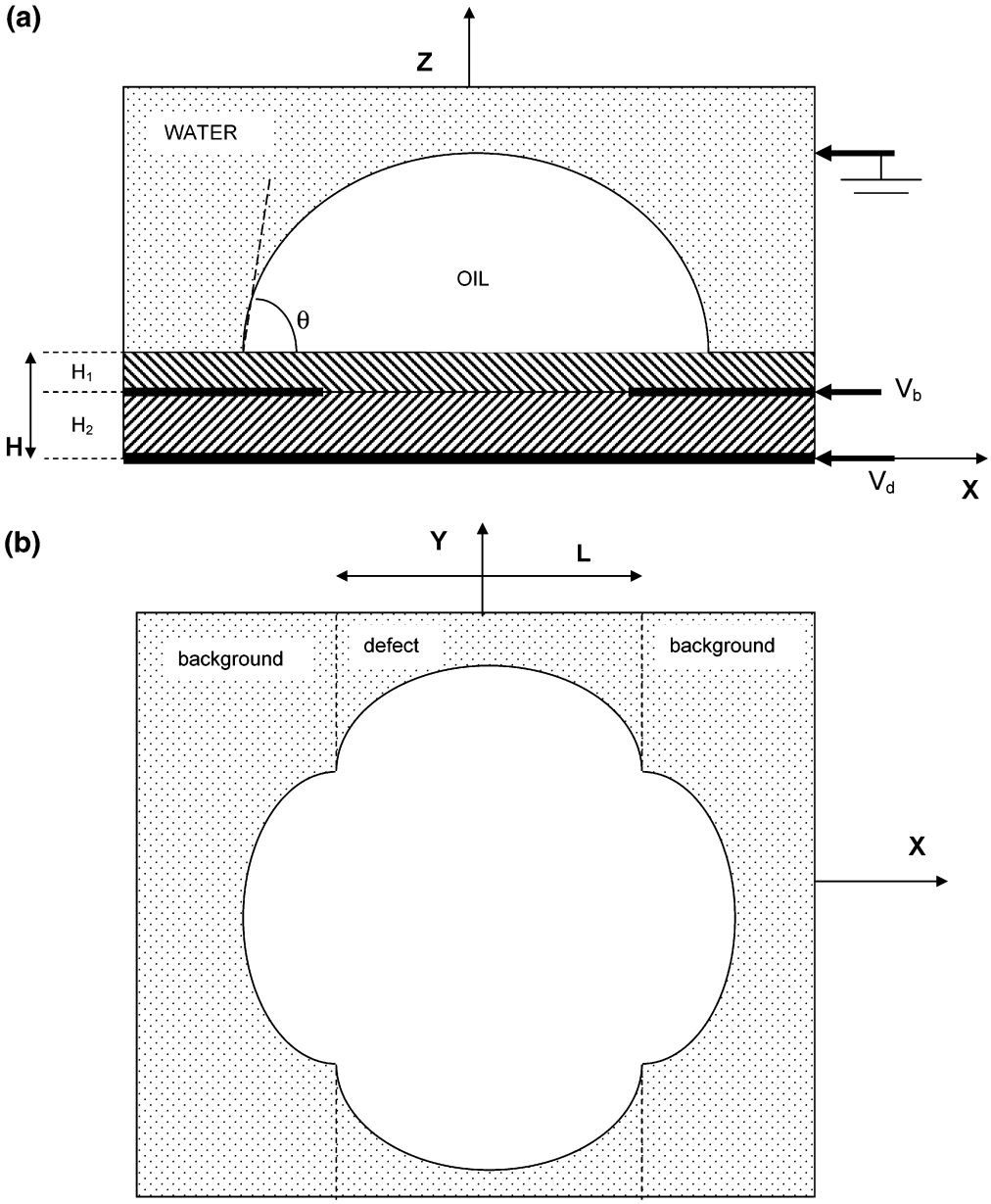

Figure 1. Sketch of the bilayered capacitor (a, side view; b, top view) used to induce an inhomogeneous solid/water interfacial energy, here mimicking a stripe-shaped defect of width L. For practical purposes, the solid insulating layer is composed of two different media with two different dielectric constants ϵ_1 (\ \ \ \) and ϵ_2 (/ / / /) and two different thicknesses H_1 and H_2. The design of the upper electrode (here at potential V_b) holds the virtual wetting geometry of the substrate: we call "background" the surface above the upper electrode and "defect" the surface under which this upper electrode is absent, here a central stripe along the y direction. The view in part b schematically represents the shape of a drop when such a defect is wetted.

Theory

The general method to determine the equilibrium shape of the oil drop in the presence of applied voltages is the minimization of the thermodynamic potential:

$$\tilde{F} = \gamma_{SW}\Sigma_{SW} + \gamma_{SO}\Sigma_{SO} + \gamma_{OW}\Sigma_{OW} - {}^1/_2\int \mathbf{E}\cdot\mathbf{D}\, dv \quad (1)$$

where the first three terms correspond respectively to the substrate/water, substrate/oil, and oil/water interfacial energies (γ are the energies per unit area, and the Σ represent the surface areas) and the last term corresponds to the electrostatic contribution.[28] A priori, the volume integral in the latter term extends to the whole space. However, for the low-frequency voltages considered in the present work, water can be considered a perfect conductor and the electric field is nonvanishing only in the insulating part of the system, that is, in the space below water and above the lower electrode (see Figure 1). It is interesting to note that, for given applied voltages, eq 1 can be rewritten as

$$\tilde{F} = \int_{\Sigma_{SW}} \gamma_{SW}(x, y)\, dx\, dy + \int_{\Sigma_{SO}} \gamma_{SO}(x, y)\, dx\, dy + \gamma_{OW}\Sigma_{OW} + C \quad (2)$$

where

$$\gamma_{SW}(x, y) = \gamma_{SW} - {}^1/_2\int_{H_e(x)}^{H} \mathbf{E}\cdot\mathbf{D}\, dz \quad (3)$$

and

(28) Landau, L.; Lifshitz, E.; Pitaevski, L. *Electrodynamics of continuous media*; Pergamon Press: Elmsford, NY, 1984.

$$\gamma_{SO}(x, y) = \gamma_{SO} - {}^1/_2\int_{H_e(x)}^{H_{OW}(x, y)} \mathbf{E}\cdot\mathbf{D}\, dz \qquad (4)$$

are the "effective" interfacial energies in the presence of the electrostatic field. The lower boundary $H_e(x)$ is the height of the higher electrode:

$$H_e(x) = H_2 \quad \text{for} \quad |x| > L/2$$
$$= 0 \quad \text{for} \quad |x| < L/2$$

$H_{OW}(x, y)$ is the height of the oil/water interface. The constant C in this equation corresponds to the electrostatic energy stored between the upper and the lower electrodes, which is, to a good approximation, independent of the spreading of the drop.

Because the thickness H of the dielectric layer is small in comparison with the oil drop thickness, most of the electrostatic energy lies in the region below the substrate/water interface and the electrostatic term in eq 4 can be neglected in a first approximation (i.e., the usual interfacial energy γ_{SO} is unmodified by electrostatic effects).

When capacitor edge effects can be neglected as well, eq 3 can be trivially put under the form

$$\gamma_{SW}(x, y) = \gamma_{SW} - {}^1/_2 c_b {V_b}^2 = \gamma_{SW}^b \quad \text{for}$$
$$|x| > L/2 \text{ (in the "background" area } \Sigma_{SW}^b)$$
$$= \gamma_{SW} - {}^1/_2 c_d {V_d}^2 = \gamma_{SW}^d \quad \text{for}$$
$$|x| < L/2 \text{ (in the "defect" area } \Sigma_{SW}^d) \quad (5)$$

where c_b is the capacitance of the insulating layer between water and the upper electrode ("background" capacitance) and c_d is the capacitance of the insulating layer between water and the lower electrode ("defect" capacitance). V_b (V_d) is the potential difference between water and the upper (water and the lower) electrode. Under these approximations the shape of the oil drop can be obtained from the minimization of

$$\tilde{F} = \gamma_{SW}^b \Sigma_{SW}^b + \gamma_{SW}^d \Sigma_{SW}^d + \gamma_{SO}\Sigma_{SO} + \gamma_{OW}\Sigma_{OW} \qquad (6)$$

at a constant solid/liquid interface area ($\Sigma_{SW}^b + \Sigma_{SW}^d + \Sigma_{SO}$ = constant) and constant drop volume. When the relation

$$c_b {V_b}^2 = c_d {V_d}^2 \qquad (7)$$

is fulfilled, it leads to $\gamma_{SW}^b = \gamma_{SW}^d$: interfacial tensions of background and defect with water are modified by the same amount through EW and the defect may be considered "canceled". Equation 6 then reduces to

$$\tilde{F} = \gamma_{SW}^b \Sigma_{SW} + \gamma_{SO}\Sigma_{SO} + \gamma_{OW}\Sigma_{OW} \qquad (8)$$

and the minimum of $\tilde{F}$ corresponds to a plane−spherical shaped drop with a unique contact angle θ given by[1,29]

$$\cos\theta = (\gamma_{SW}^b - \gamma_{SO})/\gamma_{OW} = \cos\theta_0 - {}^1/_2 c_b {V_b}^2/\gamma_{OW} \qquad (9)$$

In the other cases, the defect induces a change in the shape of the drop that can be calculated numerically by considering two different interfacial energies: one in the stripe defect (γ_{SW}^d) and the other in the background (γ_{SW}^b). The contact angle then takes two different values θ_d and θ_b in these two areas.

(29) Quilliet, C.; Berge, B. Investigation of effective interface potentials by electrowetting. *Europhys. Lett.* **2002**, *60*, 99.

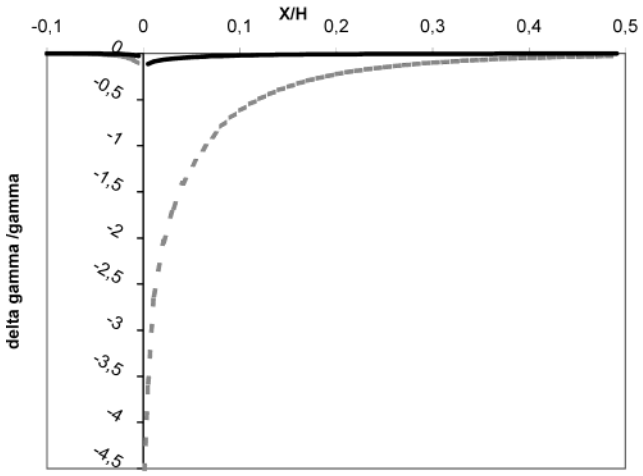

Figure 2. Contribution of the electrode edge effect to the substrate/water effective surface tension calculated using the model described in appendix A. The ordinate $\delta\gamma_{SW}/\gamma_{SW}$ corresponds to the expressions given in eqs 10a (for $x < 0$, i.e., above the upper semi-infinite electrode) and 10b (for $x > 0$, i.e., above the lower electrode) divided by the surface tension $\gamma_{SW} = 59$ mN/m of the Teflon/water interface. The abscissa is the reduced position x/H, $H = H_1 + H_2$ being the total dielectric thickness (the simulations are done here for $H_2/H_1 = 9$). The continuous dark line corresponds to $V_d = 583$ V and $V_b = 228$ V ($R = 2.56$) and the light-gray dashed line corresponds to $V_d = 400$ V and $V_b = 305$ V ($R = 0.31$). The edge effect is negligible for the case of $V_d = 696$ V, $V_b = 93$ V ($R = 6.52$).

The advantage of the present formulation of the EW effect in terms of "effective" interfacial energies (eqs 3 and 4) is to enable taking into account more refined calculations of the inhomogeneous electric field in the system. In particular, it is possible to quantify the influence of capacitor edge effects. The electric field near the edge of the upper electrode can be approximately calculated by using a simplified two-dimensional model (a semi-infinite plane electrode at potential V_b between two infinite parallel electrodes at potential 0 and V_d). The electric field can be calculated exactly in this model by using conformal mapping methods; the result is given in appendix A. Near the edges ($x \approx \pm L/2$), the effective interfacial energy is modified with respect to the infinite capacitor approximation case by an amount

$$\delta\gamma_{SW}(x, y) = -{}^1/_2[\epsilon_0\epsilon\int_{H_2}^{H} \mathbf{E}^2(x, y, z)\, dz - c_b {V_b}^2] \quad \text{for}$$
$$|x| > L/2 \quad (10a)$$

$$\delta\gamma_{SW}(x, y) = -{}^1/_2(\epsilon_0\epsilon\int_{0}^{H} \mathbf{E}^2(x, y, z)\, dz - c_d {V_d}^2) \quad \text{for}$$
$$|x| < L/2 \quad (10b)$$

(For the sake of simplicity, the same dielectric constant ϵ was taken for both insulating layers, that is, $\epsilon_1 \approx \epsilon_2 \approx \epsilon$ with notations of Figure 1.)

The first result is that there is an expected decrease of γ_{SW} in the area above the edge of the defect, that is, a dewetting tendency for the oil drop in that area, whatever the imposed voltages V_b and V_d. The variation $\delta\gamma_{SW}$ is actually logarithmically divergent for a perfectly sharp edge, but this weak divergence is rounded off in real systems.

The main interest of the model is to provide an estimate of the spatial range over which edge effects play a significant role. The electrostatic contribution to the effective surface tension is calculated by the numerical integration of $|E|^2\, dZ$ at constant x using Mathematica software; the results are shown in Figure 2 for different values of the

ratio $R = (V_d - V_b)/V_b$. One can see that the edge effect strongly depends on R. This may have a noticeable effect on the "defect" side where the edge effect extends over distances on the order of the *total* dielectric thickness H (≈0.2 mm with experimental values given in the following sections). This is an important result for practical applications because it gives clues about the sharpness of such an electrostatic defect: the extension of the transition zone between uniform γ_b and γ_d scales depends not merely on the thickness of the upper dielectric layer but in fact on the whole thickness of the bilayered condensator as a result of the long-range nature of the electrostatic forces.

Experimental Section

The sample consists of a bilayered capacitor of two glass slides covered by 500-Å ITO (indium/tin oxide, a conductive oxide square of resistance 70 Ω) glued one above the other by transparent epoxy resin Araldite 2020. On Figure 1a, the bottom glass slide corresponds to $z \leq 0$ and its ITO coating is the plane electrode represented at $z = 0$. The top glass plate (a 0.17-mm-thick cover slide, $z = 0$ to $H - H_1$) holds the wetting pattern: for the sake of demonstration, the shape of the defect is a rectangular hole (Figure 1b) of $L = 1$ mm in width and 2.5 cm in length, which is created by etching the ITO layer (at $z = H_2 = H - H_1$) via a standard lithography process. The upper dielectric layer ($z = H_2$ to H) consists of a Teflon film 25-μm thick glued on the glass slides with Araldite. To avoid the deformation of the drop due to the electrode, our experiments are performed with a drop of bromododecane surrounded by a sodium sulfate solution (subsequently referred to as "brine") acting as an electrode, both having the same volume mass of 1048 kg·m^{-3}. In such a configuration, the gravity effects are neglected and the shape of the drop is controlled solely by the surface tension and the electrostatic effects. The Teflon surface is then treated with Tetra-Etch (Gore) to create a hydrophilic ring of 1 cm in diameter that wedges the hydrophobic liquid within this perimeter. Liquids have to be contained, which is ensured by a Teflon cell clasping the substrate, thus forming a tank. The drop (of typical volume 40 μL) is observed with a CCD video camera placed above the cell. The sample, which is transparent, is lit by a parallel beam from below. Because the rays passing through the drop (which acts as a convergent lens)[30] are deflected, the drop appears black on white except for a central white spot, whose size and shape depend on the camera aperture diaphragm. Hence, we obtain a good contrast for the observation of the base or equatorial area of the deformed drop. The Teflon cell is settled on the experimental setup, which includes the image acquisition line and the computer that controls V_b and V_d, which are respectively the voltages applied to the background and the defect electrodes, the brine being electrically linked to the earth.

Results and Discussion

A potential difference is applied between the brine and the electrodes. Alternating current (ac) is chosen to avoid charge injection into the dielectric layer and, thus, scan a wider range of voltages before the system reaches EW saturation.[6,7] The ac voltage frequency separating the dielectric and conductive properties of the conducting liquid is[4,6−8]

$$f_C = \frac{\sigma}{2\pi(\epsilon_0\epsilon + CD/2)} \qquad (11)$$

where σ, ϵ, and D are respectively the conductivity, the dielectric constant, and the thickness of the brine and C is the capacitance of the system. The frequency we used is 1 kHz, which is far below the cutoff frequency order for the DEP effect in our system ($\sigma = 5$ S·m^{-1}, $\epsilon = 80$, $D = 1 \times 10^{-2}$ m, $C = 1 \times 10^{-6}$ F·m^{-2} ⇒ $f_c \approx 100$ MHz).

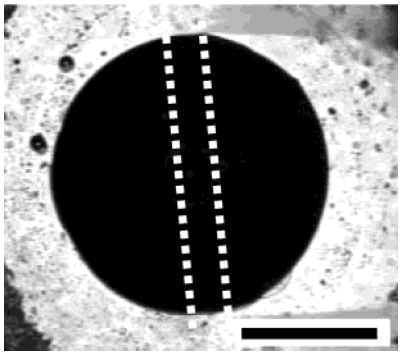

Figure 3. Oil drop (80 μL) on a "canceled defect"; scale bar = 3.4 mm. Here, $V_b = 228$ V and $V_d = 583$ V, which correspond to a contact angle of 80°. The dotted line shows the position of the defect.

By performing ramps of increasing and then decreasing tensions, we were able to determine that the base of the drop remained circular when shrinking (Figure 3) for a ratio $V_d/V_b = 2.3$. When the defect is canceled this way, the drop is assumed to be a spherical cap with a unique contact angle that may be calculated from base surface measurements, as shown in appendix B. It is then possible, by keeping this ratio constant, to draw EW curves. The latter provides a one-to-one relation between the contact angle on the background as well as on the defect area and the applied voltage, in both the case of increasing and that of decreasing voltages. Data displayed in Figure 4 present a quadratic variation of cos θ with voltage, which is in agreement with eq 1, apart from extremes: for high voltages, θ increases up to a limit where the saturation regime occurs (here 275 V, 110°). For small voltages, the oil drop is anchored on the border of the hydrophilic ring, with an initial contact angle θ_{ini} imposed by canthotaxis,[31] which is larger than the angle that would be imposed by EW on a nonetched insulator surface. When the voltage is increased, the oil drop does not begin to shrink until the voltage reaches the value V_c such as $\theta(V_c) = \theta_{ini}$ for increasing voltage (for the experiments displayed in Figure 4, $\theta_{ini} = 30°$ and $V_c = 75$ V). A point that is still unclear is that, as often is the case in EW experiments, the background capacitance extracted from the EW curves (12×10^{-7} F·m^{-2}) does not match the direct capacimetric measurements (4.4 10^{-7} F·m^{-2}). For the moment, there is little theoretical work to explain this kind of discrepancy.[32]

We then tuned the background and defect voltages and observed that the oil drop shape could be continuously modified between two extreme situations (Figure 5A,C), where the stripe acts qualitatively as a wetting or a nonwetting defect. To study these defects somewhat more quantitatively, the equatorial drop shapes were compared with Surface Evolver simulations made for a sessile drop riding a striped defect. In these simulations, there is a sharp transition between the defect where the drop has a contact angle θ_d and the background with a contact angle θ_b. The contact angles imposed in the simulation were deduced from the EW hysteresis curves of Figure 4. The strength of the defect $\Delta\gamma = \gamma_{SW}^d - \gamma_{SW}^b$ is then calculable

(30) Peseux, J.; Berge, B. Variable focal lens controlled by an external voltage: an application of electrowetting. *Eur. Phys. J. E* **2000**, *3*, 159.

(31) Domingues Dos Santos, F.; Ondarçuhu, T. Ancrage d'un liquide sur une discontinuité chimique de surface. *J. Chim. Phys.* **1996**, *93*, 1991.

(32) Quinn, A.; Attard, P. Stray capacitance contribution to the electrical measurement of contact angles and areas. *Rev. Sci. Instrum.* **2003**, *74*, 2517.

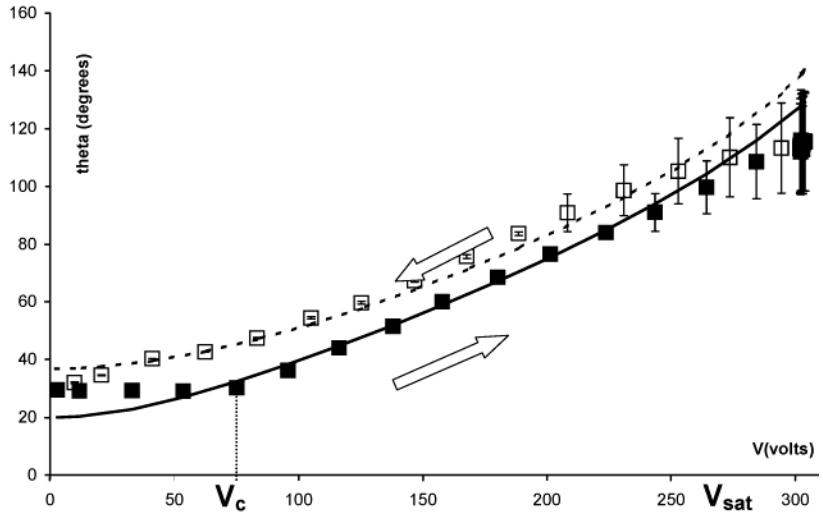

Figure 4. EW hysteresis curve: contact angle versus voltage (here V_b), full squares corresponding to increasing voltage and hollow squares to decreasing voltage. The theoretical curves (full line for increasing voltage, dotted line for decreasing voltage) are calculated according to eq 5 with $C_b = 12 \times 10^{-7}$ F·m^{-2} and present a shift at 0 voltage that indicates a contact angle hysteresis of 17° for the substrate surface. The apparent inaccuracy between the experimental and the theoretical curves for $V < 75$ V and $V > 275$ V is discussed in the text. To obtain the angle as a function of the voltage for V_d, the same curve is to be plotted with voltages on the x axis multiplied by the ratio $V_d/V_b = 2.3$ corresponding to the "cancellation" of the defect. The defect capacitance extracted from the curves is then $C_d = 1.8 \times 10^{-7}$ F·m^{-2} (direct capacimetric measurement $C_d = 2.5 \times 10^{-7}$ F·m^{-2}).

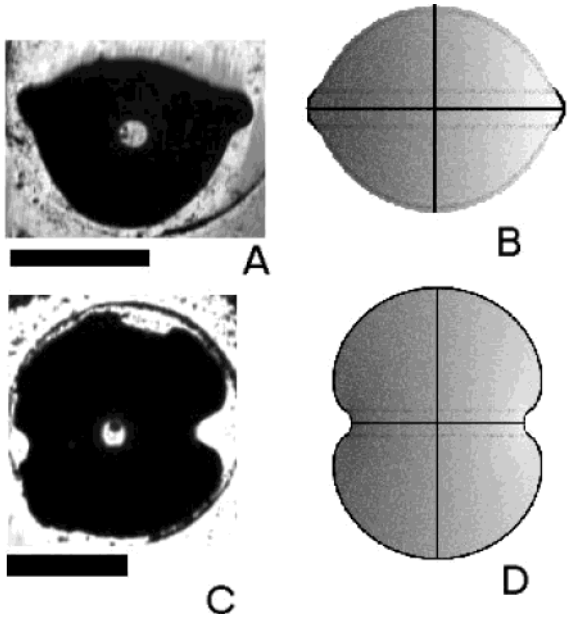

Figure 5. Same oil drop on a bilayered substrate with two different sets of voltages applied to the electrodes, mimicking a wetting (A) and a dewetting (C) stripe; scale bar = 5 mm. The corresponding Surface Evolver simulations (B and D) are performed with contact angles deduced from the EW curves of Figure 4. (A and B) Slowly increasing voltages $V_b = 305$ V and $V_d = 400$ V ($R = 0.31$). Simulation with contact angles 107 and 64° respectively for background and defect. (C and D) $V_b = 93$ V (slowly decreasing) and $V_d = 696$ V ($R = 6.52$). Simulation with contact angles 45 and 106° respectively for background and defect.

from both contact angles, through eqs 5 and 9, which lead to

$$\Delta\gamma = \gamma_{OW}(\cos\theta_d - \cos\theta_b) \qquad (12)$$

Let us notice that the hysteresis is about 17°, a value reproducible in our experiments but higher than the one reported in previous works;[30,33] this is probably due to the industrial Teflon film quality, which is highly dependent on the batch. However, a low hysteresis is not needed in our experiments: if the voltages are kept slowly and monotonically varying (<0.5 V·s^{-1}), the contact angle is deducible from the EW curves.

The shapes simulated as indicated (Figure 5B,D) are qualitatively comparable to the experimental pictures, taking into account the fact that in the nonwetting case (Figure 5C) an important part of the contact line is pinned on the hydrophilic ring border. Apart from this situation, the average contact angle values extracted from the EW curves performed with a "canceled defect" are likely to reflect real values that cannot be measured directly in the case of a noncanceled defect. We were able to obtain a defect strength $\Delta\gamma$ varying from $-\gamma_{OW}$ to $^2/_3\gamma_{OW}$, which is comparable to performances of "real" wetting defects.[34] Last, it is interesting to note that in both the experimental situations, the drop "follows" the defect slightly better than in the simulations, as if the wettability contrast was enhanced at the defect border. The edge effect displayed on Figure 2 qualitatively agrees with this observation in the wetting case but cannot be invoked for the nonwetting case (negligible for $R = 6.52$). A possible explanation is that the model presented in this paper does not take into account the water wedge at the water/oil/substrate triple line and the consecutive deformation of the field at its vicinity. This is much more difficult to calculate analytically, but we can expect a sharp-edge electrostatic attraction between the water wedge and the oppositely charged upper electrode border, tending to make them parallel to each other. Such an effect could sharpen the drop profile discontinuity at the defect boundaries, thus apparently increasing the wettability contrast between the background and the EW defect.

Conclusion

In an attempt to use EW to alter the wetting properties of an hydrophobic substrate nonuniformly, our experi-

(33) Janocha, B.; Bauser, H.; Oehr, C.; Brunner, H.; Göpel, W. Competitive electrowetting of polymer surfaces by water and decane. *Langmuir* **2000**, *16*, 3349.

(34) De Gennes, P.-G.; Brochard-Wyart, F.; Quéré, D. *Gouttes, bulles, perles et ondes*; Belin: Paris, France, 2002.

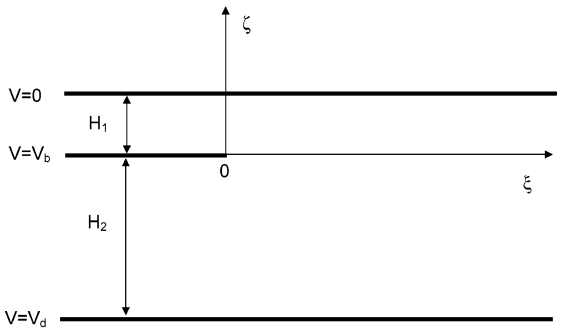

Figure 6. Geometry of the three electrodes (in bold) used for the electrostatic calculations of the edge effect (appendix A).

ments proved the feasibility of controlling the strength of wetting defects through the electrical voltage with a bilayered capacitor device. The deformation of sessile drops shows that these defects can be continuously tuned wetting or nonwetting with a strength comparable to classical defects, including the intermediate case where wetting uniformity is recovered ("canceled defect"). To evaluate the specificity of such "electrowetting" defects, we developed a model showing that electrostatic edge effects are expected to limit the defect sharpness, which depends on the whole capacitor thickness. The latter point is particularly important for microfluidic purposes because miniaturization will require a drastic (and reliable) diminution of the total insulator thickness.

Acknowledgment. We thank Patrice Ballet for the high-tension monitoring device and Marc Fermigier for guiding us toward Surface Evolver and providing the subroutine.

Appendix A: Edge Effect

To estimate the importance of the edge effect, we consider the electrostatic system that consisted of an infinite parallel plane capacitor of thickness H with a semi-infinite plane electrode laying inside (see Figure 6). The electrostatic potentials of the three electrodes are respectively $V = 0$, V_b, and V_d. We put $R = (V_d - V_b)/V_b$ and $r = H_1/H_2$.

The electric field in this two-dimensional system can be exactly calculated using conformal mapping methods.[35] The transformation that maps the stripe ($-\infty < u < \infty$, $0 \le v \le \pi$) of the (u, v) complex plane into the stripe ($-\infty < \xi < \infty$, $-H_2 \le \zeta \le H_1$) of the (ξ, ζ) complex plane with a branch cut along ($-\infty < \xi < 0$) is

$$\xi + i\zeta = -(H_2/\pi)\{u + iv + (1+ r) \ln[(r + \exp(-u - iv))/(1 + r)]\} \quad \text{(A1)}$$

In this transformation, the upper electrode ($-\infty < \xi < \infty$, $\zeta = H_1$) corresponds to ($-\infty < u < -\ln(r)$, $v = \pi$), the lower electrode ($-\infty < \xi < \infty$, $\zeta = -H_2$) to ($\infty > u > -\ln(r)$, $v = \pi$), and the intermediate electrode ($-\infty < \xi < 0$, $\zeta = 0$) to ($-\infty < u < \infty$, $v = 0$). A vertical line at ξ corresponds to

$$\cos(v) = \{(1 + r)^2 \exp[-(2\pi\xi/H) + u(r - 1)/(r + 1)] - \exp(-u) - r^2 \exp(u)\}/(2r) \quad \text{(A2)}$$

The components E_X and E_Z of the electric field are found to be given by

$$E_X - iE_Z = -i(V_b/H_1)[1 - rR \exp(u + iv)]/[1 - \exp(u + iv)] \quad \text{(A3)}$$

After a few lines of calculation, one can show that

$$\int \mathbf{E}^2(\xi, \zeta)\, d\zeta = V_b^2/(\pi r H) \int [\exp(-u) - 2rR \cos(v) + (rR)^2 \exp(u)]/\sin(v)\, du \quad (4)$$

From eqs 10, A2, and A4, one can calculate $\delta\gamma(\xi)$, the electrostatic contribution to the effective surface tension, by numerical integration. The results are shown in Figure 2.

As a result of the edge effect, $\delta\gamma(\xi)$ shows a logarithmic divergence when ξ goes to 0:

$$\delta\gamma(\xi) \approx \epsilon_0 \epsilon V_b^2 (1 - rR)^2/(4\pi r H) \ln[2\pi\xi(1 + r)^2/(rH)] + cst \quad \text{(A5)}$$

One notes that this divergence disappears when $rR = 1$: the electric field is then uniform in the whole capacitor and edge effects vanish.

Appendix B: Contact Angle Calculations

Consider a spherical cap, with volume V on a solid with a contact angle θ between the liquid and the solid. Depending on the value of θ, we have the following:

(1) $\theta < 90°$. The surface S seen from above is the contact surface between the drop and the solid. Consequently, the relation between S and $\cos\theta$, based upon geometrical relations, is[36]

$$\cos\theta = -1 + \frac{\alpha^2}{\beta} + \frac{\alpha\beta}{4 + \alpha^3} \quad \text{(i)}$$

with

$$\alpha = \frac{S}{\pi^{1/3}(^3/_2 V)^{2/3}}$$
$$\beta = [16 + 8\alpha^3 + \alpha^6 + 2(4 + \alpha^3)^{3/2}]^{1/3} \quad \text{(ii)}$$

(2) $\theta > 90°$. The surface S seen from above is the equatorial surface of the drop. The expression of the volume of the drop depending on $\cos\theta$ leads to a third-degree equation for $\cos\theta$. Only one solution lies within the range of a cosine:

$$\cos\theta = \frac{-x_0 + \sqrt{\Delta}}{2} \quad \text{(iii)}$$

with

$$x_0 = 2\cos\left(\frac{1}{3}\arctan\frac{\sqrt{4 - q^2}}{q}\right)$$
$$q = 2 - \frac{3V\sqrt{\pi}}{S^{3/2}} \quad \text{(iv)}$$
$$\Delta = x_0^2 + 4(q/x_0)$$

LA030079W

(35) Lavrentiev, M.; Chabat, B. *Méthodes de la théorie des fonctions d'une variable complexe*; Editions Mir: Moscou, France, 1977.

(36) Verheijen, H. J. J.; Prins, M. W. J. Contact angle and wetting velocity measured electrically. *Rev. Sci. Instrum.* **1999**, *70*, 3668.